The Journal of Chemical Physics

RESEARCH ARTICLE | MAY 15 2024

The initial sticking of high velocity water onto graphite under non-equilibrium supersonic flow conditions

Kevin D. Gibson ; Yuheng Luo ; Christopher Kang ; Rui Sun ; Steven J. Sibener

J. Chem. Phys. 160, 194705 (2024)
https://doi.org/10.1063/5.0205984

AIP Publishing

The Journal of Chemical Physics ARTICLE pubs.aip.org/aip/jcp

The initial sticking of high velocity water onto graphite under non-equilibrium supersonic flow conditions

Cite as: J. Chem. Phys. 160, 194705 (2024); doi: 10.1063/5.0205984
Submitted: 28 February 2024 • Accepted: 26 April 2024 •
Published Online: 15 May 2024

Kevin D. Gibson,[1] Yuheng Luo,[2] Christopher Kang,[2] Rui Sun,[2] and Steven J. Sibener[1,a)]

AFFILIATIONS

[1] The James Franck Institute and Department of Chemistry, The University of Chicago, 929 East 57th Street, Chicago, Illinois 60637, USA
[2] Department of Chemistry, University of Hawaii at Manoa, 2545 McCarthy Mall, Honolulu, Hawaii 96822, USA

Note: This paper is part of the JCP Special Topic on Water: Molecular Origins of its Anomalies.
[a)] **Author to whom correspondence should be addressed:** s-sibener@uchicago.edu

ABSTRACT

In this paper, we present a combined experimental and theoretical study that explored the initial sticking of water on cooled surfaces. Specifically, these ultra-high vacuum gas–surface scattering experiments utilized supersonic molecular beam techniques in conjunction with a cryogenically cooled highly oriented pyrolytic graphite crystal, giving control over incident kinematic conditions. The D_2O translational energy spanning 300–750 meV, the relative D_2O flux, and the incident angle could all be varied independently. Three different experimental measurements were made. One involved measuring the total amount of D_2O scattering as a function of surface temperature to determine the onset of sticking under non-equilibrium gas–surface collision conditions. Another measurement used He specular scattering to assess structural and coverage information for the interface during D_2O adsorption. Finally, we used time-of-flight (TOF) measurements of the scattered D_2O to determine how energy is exchanged with the graphite surface at surface temperatures above and near the conditions needed for gaseous condensation. For comparison and elaboration of the roles that internal degrees of freedom play in this process, we also did similar TOF measurements using another mass 20 incident particle, atomic neon. Enriching this study are precise molecular dynamics simulations that elaborate on gas–surface energy transfer and the roles of molecular degrees of freedom in gas–surface collisional energy exchange processes. This study furthers our fundamental understanding of energy exchange and the onset of sticking and ultimately gaseous condensation for gas–surface encounters occurring under high-velocity flows.

INTRODUCTION

The heterogeneous nucleation of water on solid surfaces is of great economic and ecologic interest and has been widely studied.[1] Nucleation begins with the initial sticking of the water molecules on a surface with little, if any, adsorbed water, which is what we will investigate in this paper. Previous work includes both theoretical examinations,[2] the role of surface defects in the adsorption of water on the face of a crystal,[3] and the initial formation of clouds and raindrops.[4] In this study, we experimentally investigated the precursor to nucleation—the initial sticking of D_2O on surfaces. The experiments were performed in a vacuum chamber under highly controlled conditions to allow for a separate evaluation of the importance of each of the parameters in initiating water sticking. This was facilitated by the use of molecular beam techniques, allowing us to explore the initial sticking as a function of incident energy (E_I), incident angle (Θ_I), incident flux (Φ_I), and surface temperature (T_S). The surface used highly oriented pyrolytic graphite (HOPG), which, when clean, is hydrophobic or slightly hydrophilic.[5] (Hydrophobic corresponds to a contact angle >90°, hydrophilic to a contact angle <90°.) HOPG was chosen due to its level of perfection and many known aspects of water interactions with this model surface. It represents the first examination of water scattering and condensation with high translational energies in a non-equilibrium regime, a substantial expansion of previous work at lower scattering energies.[10,11]

For sticking to occur, enough of the incident energy must be exchanged with the surface such that the molecule can be trapped in the surface potential well, ~100 meV.[6] At the surface temperature at which adsorption begins, there can also be appreciable desorption, so the temperature at which there is net adsorption can vary with incident flux. The surface temperature can also have an effect on the surface mobility of an adsorbate; at lower temperatures, the molecule may be immobile on the surface, while at higher surface temperatures, the molecule may still be bound to the surface in the normal direction but have sufficient energy to overcome the activation barrier for diffusion across the surface. Flux can then become important, even in the case of transient adsorption. If two or more water molecules encounter one another before desorption, it is possible that assemblages of water molecules can form that stabilize the adsorption. Such is the case for the formation of water dimers on graphite.[7] An increased incident flux would increase the probability of such encounters.

Three different types of experiments are described. The first involved measuring He specular scattering as the surface was exposed to the D_2O. This can give information about the surface temperature at which molecules are initially adsorbed on the surface, as well as information about how the molecules are distributed; in analogy to gas phase scattering, an atom impacting near an adsorbed molecule will be scattered at an angle different than specular.[8] The second was similar to that described by King and Wells,[9] where the total amount of D_2O scattered was measured. At the temperature at which adsorption begins, the D_2O signal detected decreases. Finally, we also made some dynamical measurements, where both the angular intensity and energy distribution of the scattered D_2O were measured, an extension of the measurements of Miyoshi *et al.*[10] and Marković *et al.*[11] For comparison, we also made measurements using Ne in place of D_2O. This provides information about energy accommodation and the role of molecular internal degrees of freedom on the surface. Dynamical information is further elucidated by comparison of the experimental results with realistic and highly accurate molecular dynamics (MD) simulations; excellent agreement is found between the experimental and simulation outcomes.

EXPERIMENTAL

These experiments were performed in an ultra-high-vacuum (UHV) chamber (base pressure ~5×10^{-9} Torr for these studies), shown schematically in Fig. 1 and also described in Gibson *et al.*[12] Briefly, there is the diffusion-pumped region where the molecular beam is produced. The beam passes through several differentially pumped regions before entering the main chamber. Inside the UHV chamber, the beam impinges on the target that is mounted on a rotatable manipulator, allowing the incident angle (Θ_I, measured from the surface normal) to be varied. Any molecules leaving the surface can be detected by a differentially pumped quadrupole mass spectrometer (QMS) with a detection acceptance angle of ~ 1°. The angle of this detector relative to the surface normal (Θ_F) can be independently varied. There is also a residual gas analyzer (RGA) in the chamber that is not in the line of sight of the target.

The molecular beam is made by the expansion of a carrier gas containing gaseous D_2O at a stagnation pressure of 30–50 psig through a pinhole, typically at 35–50 μm and heated to at least 373 K,

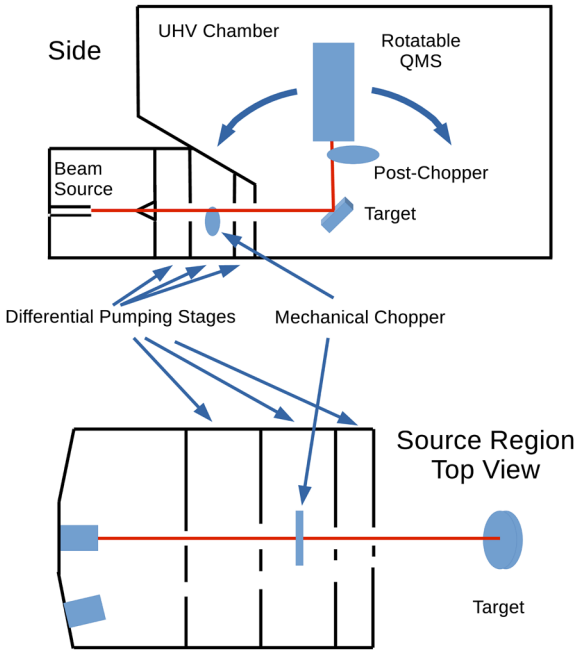

FIG. 1. Schematic of the machine used in these experiments.

into the vacuum of the first region. For these experiments, D_2O was used because the detector had an appreciable H_2O background. The D_2O is held in a reservoir through which the carrier gas is bubbled before reaching the nozzle containing the pinhole. The reservoir can be heated to increase the vapor pressure, typically at 40 °C, giving a vapor pressure of ~50 Torr, and the nozzle can be separately heated to a higher temperature to prevent condensation or any clustering in the beam and for some control of the translational energy of the D_2O. For further control of the beam energy, various carrier gases can be used: He and H_2 to make fast beams, and N_2 to make a much slower beam. To characterize the beam, the manipulator can be lowered out of the beam path, and the QMS detector can be rotated directly into the beam path. A mechanical chopper modulates the beam so that the energy distribution of the D_2O can be measured using time-of-flight (TOF) techniques. This measurement also allows for determining the relative flux of different D_2O beams used over the course of these experiments. The flux measured by this method gives us Φ_N; the flux at the surface is then $\Phi_I = \Phi_N^* \cos(\Theta_I)$.

The target crystal was ZYA HOPG graphite, which was initially cleaned by exfoliating the surface with scotch tape a few minutes before the main chamber was pumped down. The stage on which this crystal was mounted could be resistively heated and cryogenically cooled. Once pumped down, the crystal was annealed at 700 K for a few days until the He reflectivity had stabilized. The FWHM of the He specular was ~11°, in good agreement with Miyoshi *et al.*[10] We also reproduced their 63 meV D_2O scattering to help confirm the quality of the HOPG surface.

The He specular scattering as a function of the surface temperature was measured using the QMS detector with $\Theta_I = \Theta_F = 45°$. The HOPG sample had appreciable specular scattering, and even a

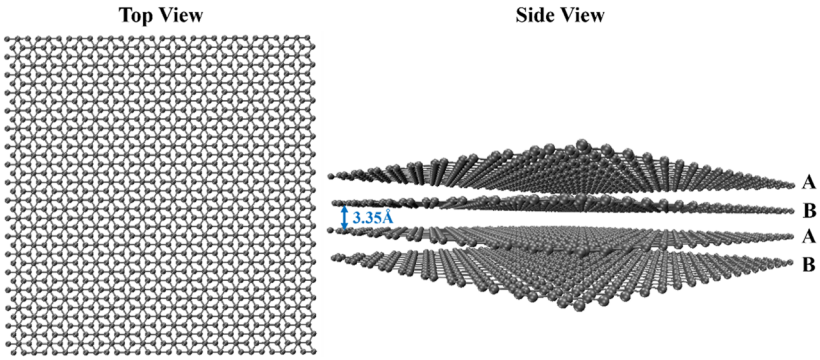

FIG. 2. Top and side view of the four-layer graphite model.

small amount of adsorbed D_2O caused a significant change in the specular intensity.[8,13] Post-exposure, temperature programmed desorption (TPD) measurements were performed to determine how much D_2O had been adsorbed on the surface. This was performed by linearly ramping the surface temperature (10 K/min.) while monitoring the D_2O signal with the QMS detector. The second set of experiments involved a measurement similar to that of King and Wells.[9] The beam was modulated by a shutter in the third differential pumping region, and the total amount of D_2O scattered from the sample could be monitored by the RGA that was not in line of sight with the HOPG target. With the shutter closed, the chamber background was determined. When the shutter is opened, the RGA signal increases due to the scattering from the HOPG surface. As T_S is progressively lowered, some of the D_2O is adsorbed, and the scattered signal decreases. Finally, we made some TOF measurements of scattered D_2O to determine the energy accommodation between the beam and the surface and to determine the angular intensity distribution. This was performed with a continuous D_2O beam that was scattered from the HOPG surface and was then modulated by the post-chopper and the signal detected by the QMS. This allows for both determining the D_2O flight time over a known distance and the relative D_2O intensity. These last experiments were compared with realistic molecular dynamics calculations to be described in the next section.

THEORETICAL METHODS AND COMPUTATION

The potential energy function for D_2O + graphite is given by

$$V_1 = V_{graphite} + V_{D2O} + V_{D2O+graphite}, \tag{1}$$

where $V_{graphite}$ is the graphite potential, V_{D2O} is the D_2O potential, and $V_{D2O+graphite}$ is the D_2O + graphite intermolecular potential.

The potential energy function for Ne + graphite is expressed by

$$V_2 = V_{graphite} + V_{Ne+graphite}. \tag{2}$$

The graphite model comprises four layers stacked in an AB sequence and is depicted in Fig. 2. The first layer (A) and the third layer are aligned, while the second layer (B) is offset, aligning the fourth layer. $V_{graphite}$ is characterized by several key components: harmonic oscillations between carbon–carbon (C–C) bonds, bending of C–C–C valence angles, torsional angles of C–C–C–C dihedral, and Lennard-Jones (L-J) (6-12) van der Waals forces for carbon atoms separated by four or more bonds. Additionally, the L-J (6-12) van der Waals forces account for interactions between carbon atoms located on different layers, with a cutoff distance of 12 Å. The parameters defining the graphite potential are derived from the OPLS-AA force field,[14] as detailed in Table 1 of Ref. 15. This potential was used in the previous N_2 + graphite simulation.[15]

The D_2O potentials (V_{D2O}) are described by a Morse function with parameters D_e = 125.6 kcal/mol, β_e = 2.19 $Å^{-1}$, and r_e = 0.957 Å, and a harmonic angle potential with parameters θ_0 = 104.52° and k_θ = 0.688 mydn Å/rad^2.[16] The intermolecular interactions between D_2O + graphite ($V_{D2O+graphite}$) and Ne + graphite ($V_{Ne+graphite}$) are described by the L-J (6-12) van der Waals potential of the following form:

$$V_{ij}^{6-12} = 4\varepsilon_{ij}\left(\left(\frac{\sigma_{ij}}{r_{ij}}\right)^{12} - \left(\frac{\sigma_{ij}}{r_{ij}}\right)^{6}\right), \tag{3}$$

where ε_{ij} and σ_{ij} represent the potential energy depth and position, respectively, and r_{ij} is the distance between atom i and atom j. The L-J (6-12) parameters for different types of atoms are calculated by the combination rules,

$$\varepsilon_{ij} = \sqrt{\varepsilon_i \times \varepsilon_j}, \tag{4}$$

$$\sigma_{ij} = \sqrt{\sigma_i \times \sigma_j}. \tag{5}$$

The L-J (6-12) parameters are summarized in Table I.

The initial sampling of the D_2O and Ne molecules was performed with the chemical dynamics program VENUS.[20,21] The initial conditions for the trajectories were chosen to model the experimental conditions. The collision energies (E_I) in the experiment were fitted with a normal distribution function

$$I(E_I) = e^{\frac{-(E_I-\mu)^2}{2\times\sigma_{std}^2}}, \tag{6}$$

with fitting parameters mean (μ) and standard deviation (σ_{std}), which were further used to perform inverse transform sampling and

TABLE I. Parameters for the Lennard-Jones (6-12) potentials.

Atom	C	O	H	Ne
ε (kcal/mol)	0.070[a]	0.273[b]	0.085[b]	0.074[c]
σ (Å)	3.550[a]	3.060[b]	1.875[b]	2.782[c]

[a]Obtained from CHARMM force field.[17]
[b]Obtained from modified TIP3P force field.[18]
[c]Obtained from previous theoretical study.[19]

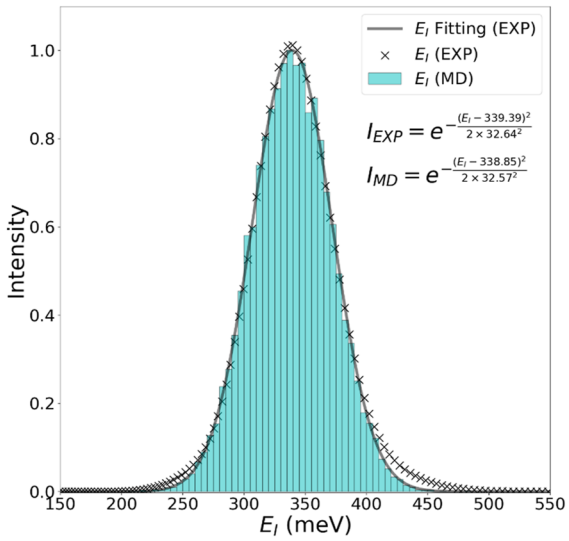

FIG. 3. The distribution of collision energies in experiments and MD simulations.

TABLE II. Initial conditions of D_2O and Ne molecules.

Molecules	D_2O			Ne	
T_{vib} (K)	373	373	373	···	···
T_{rot} (K)	23	23	23	···	···
θ_I (°)	20	40	60	20	40
μ (meV)	339.02	338.85	339.11	337.64	351.65
σ_{std} (meV)	32.53	32.57	32.82	19.83	21.42
Trajectories	20 000	20 000	20 000	20 000	20 000

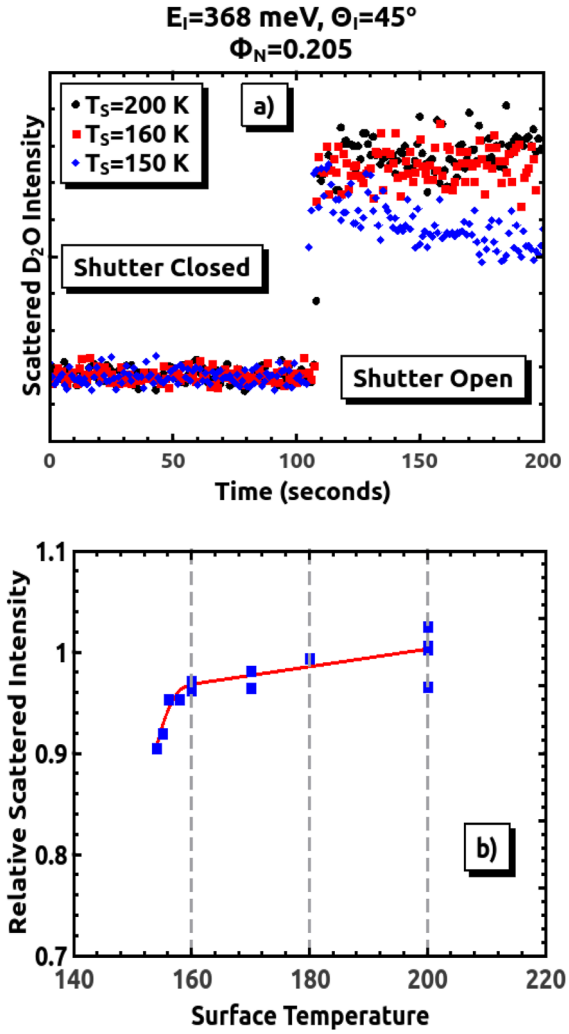

FIG. 4. Panel (a) shows the results of three King and Wells type experiments, where the total D_2O scattering intensity is measured. Panel (b) is the summary of a series of experiments, where the relative intensity is the difference between the D_2O signal when the beam is blocked and when it is allowed to impinge on the HOPG sample.

generate a distribution of collision energies for MD simulations. Figure 3 showcases the collision energies from the experiment and MD simulations.

The incident angle θ_I was defined by the angle between the initial velocity vector of the gas and the surface normal, and the beam of colliding gaseous molecules was randomly directed within a circular area with a 2.2 Å radius, ensuring it encompassed a hexagonal unit cell on the graphite surface. The beam was positioned ~40 Å above the graphite surface, and the direction in which the beam spread across the surface was determined by an azimuthal angle χ_I, which was randomly selected from any angle between 0° and 360°, ensuring uniform coverage. The vibrational and rotational energies of D_2O molecules were generated according to a Boltzmann distribution at temperatures of 373 and 23 K, respectively, to match the experiment. The initial conditions in MD simulations of D_2O and Ne molecules are summarized in Table II.

The initial sampling of the graphite surface was carried out with another chemical dynamics program, GROMACS.[22] The graphite sheet is periodic and centered in a box of ~4.5 × 4.5 × 400 nm^3. Periodic boundary conditions (PBC) were employed in all directions. After the initial 5000 steps of steepest descent minimization, the graphite surface was equilibrated under the NVT ensemble for 50 ns with a timestep of 1 fs, maintained at a temperature of 300 K using the V-rescale thermostat[23] every 0.1 ps. The cutoff distance for the short-range nonbonded interactions is 1.2 nm, with electrostatic interactions calculated using a plain cutoff with a pair list. The

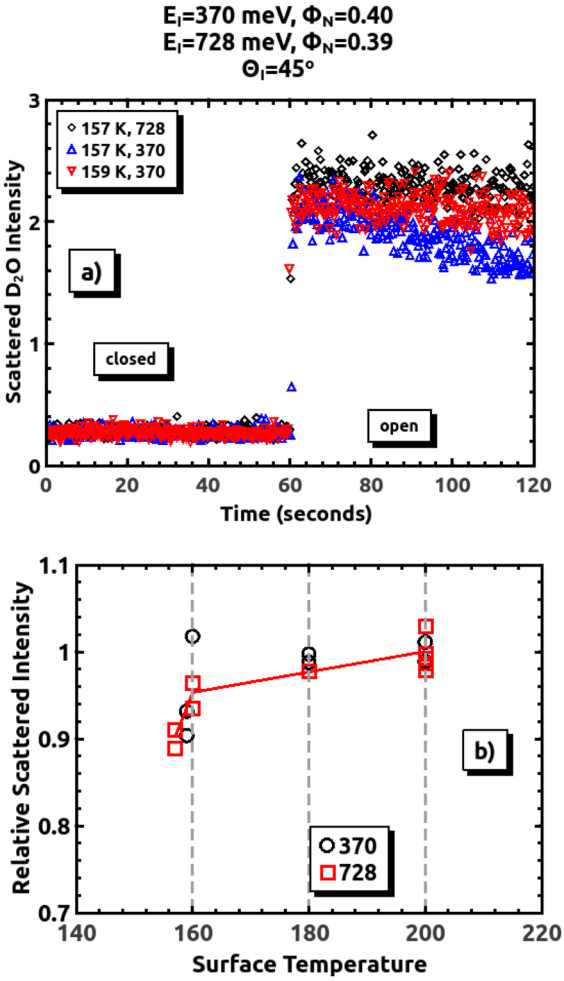

FIG. 5. Comparison of the King and Wells results for D_2O beams with the same flux but different incident energies.

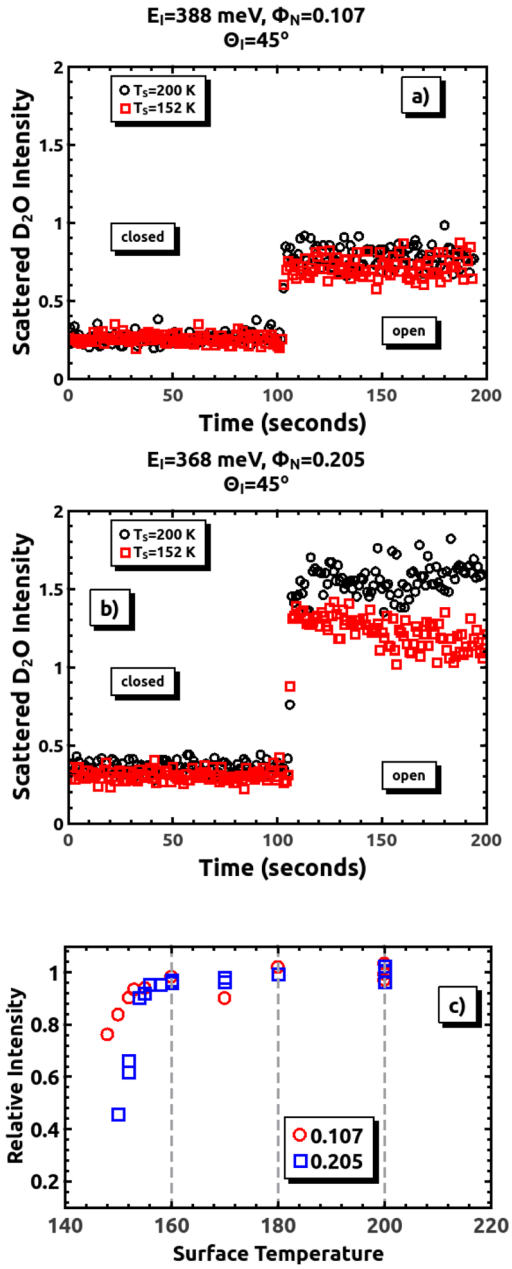

FIG. 6. Comparison of the King and Wells results for D_2O beams with nearly the same incident energy but different fluxes.

positions and velocities of all carbon atoms in the last 20 000 frames of graphite surface were saved into a graphite library (Graphite 1, Graphite 2, . . ., Graphite 20 000).

For each trajectory, molecules from a gas library were randomly paired with a graphite surface from the graphite library. A total of 20 000 trajectories were simulated for each ensemble of initial conditions (E_I, θ_I). These trajectories were propagated using the leap-frog algorithm,[24] with a timestep of 1 fs. A trajectory was terminated if the vertical distance between the center of the gas and the surface exceeded 100 Å or if the total integration time surpassed 20 ns.

The leaving angle θ_F of gaseous molecules was determined by the angle between the final velocity vector and the surface normal. The final azimuthal angle χ_F was defined by the final velocity vector's orientation relative to the scattering plane. It is noteworthy that only in-plane leaving gas with minimal χ_F values could be detected in the experiment. To derive a meaningful final angular distribution $P(\theta_F)$ from MD simulations for direct comparison with experimental data, an acceptance criterion for the final azimuthal angle $\Delta\chi_F$ was employed to determine whether the leaving gas was in-plane or out-of-plane,

$$\Delta\chi_F = \frac{l_E}{2r\,\sin\theta_F} \times \frac{180^\circ}{\pi}, \tag{7}$$

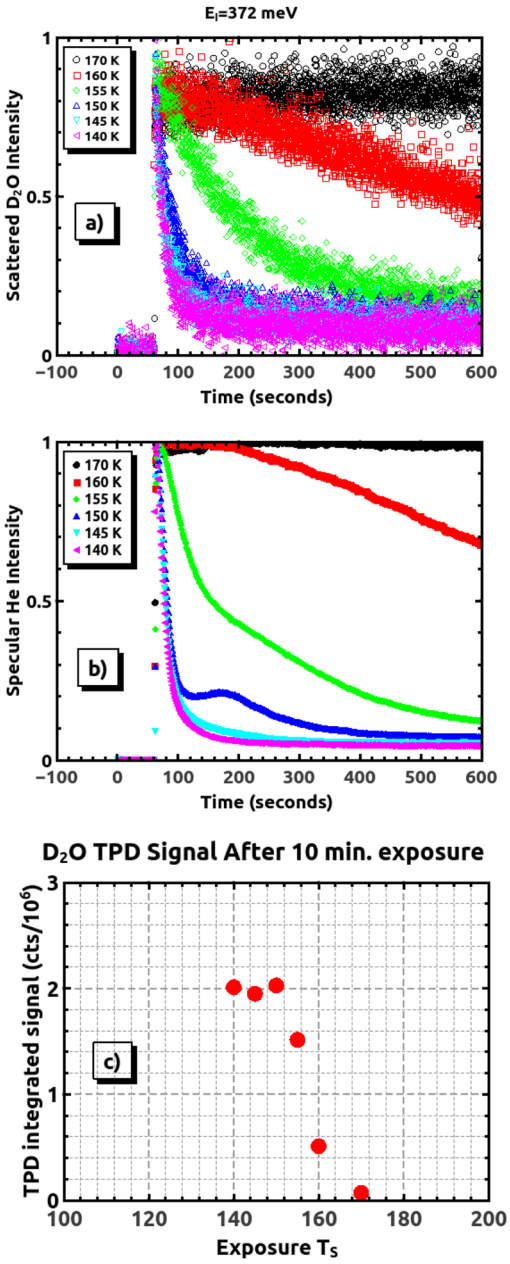

FIG. 7. Panel (a) shows the D_2O scattering at different surface temperatures, and panel (b) shows the concurrent He specular signal. Panel (c) is the result of TPD measurements made immediately after the exposure to determine the relative amount of D_2O adsorbed.

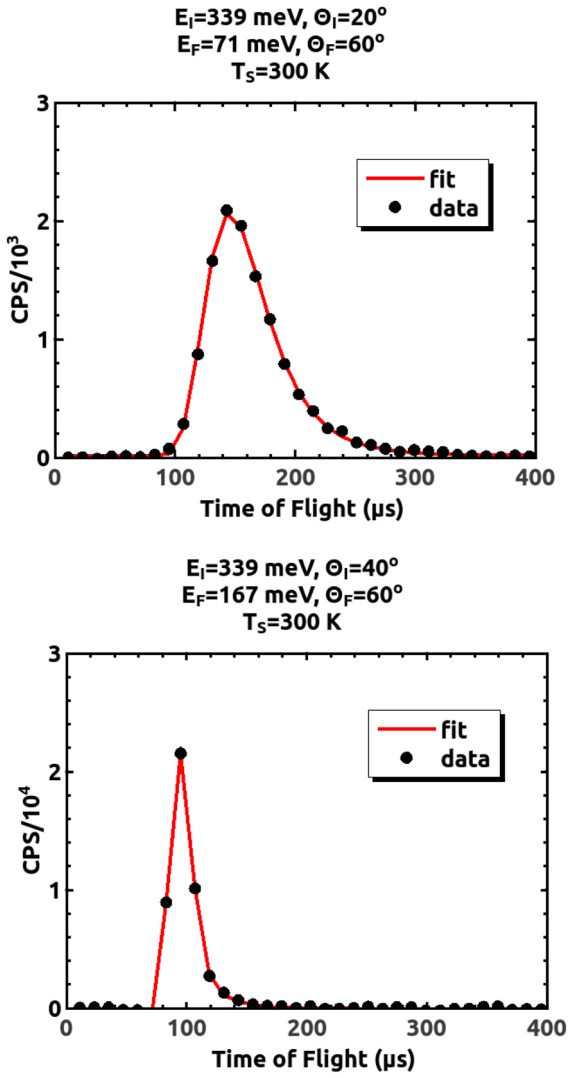

FIG. 8. Example TOF spectra and their fits.

where l_E is the diameter of the experimental aperture for capturing the leaving gas, and r is the distance between the collision center and the experimental aperture. With the experimental setup (l_E = 0.16 cm, r = 4.63 cm), the acceptance criterion $\Delta\chi_F$ is $\pm\frac{1^\circ}{\sin\theta_F}$.

The partitioning of the kinetic energy of the leaving gas was calculated directly from the positions and velocities of each atom at the x, y, and z directions. The methods of computing finial translational energy (E_{trans}), rotational energy (E_{rot}), and vibrational energy (E_{vib}) followed the protocol of classical mechanics provided in the Supplementary Information of Ref. 25.

RESULTS AND DISCUSSION

We will first discuss the square-wave modulated experiments similar to those of King and Wells.[9]

Figure 4(a) shows example results for the total D_2O scattering as measured with the RGA. There are superimposed results for three different surface temperatures. Starting at T_S = 200 K, where there is

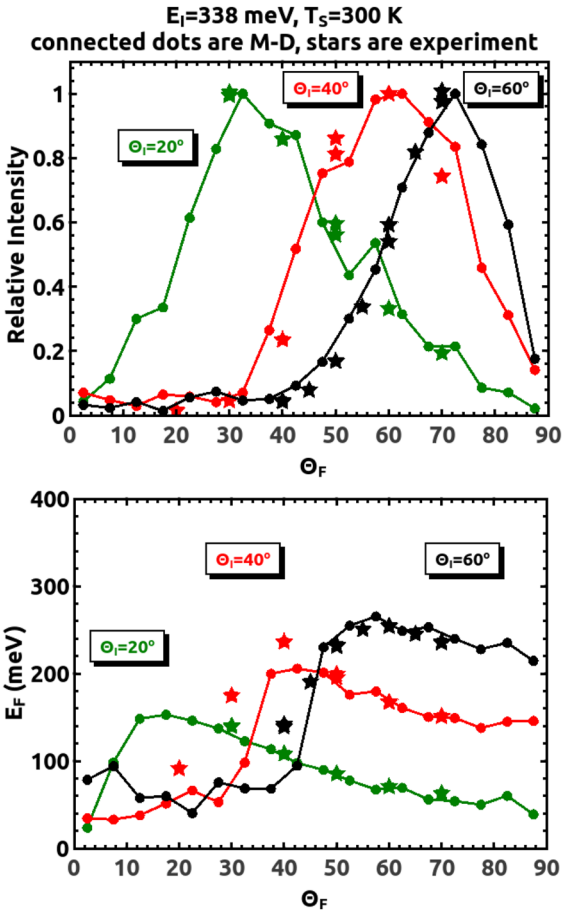

FIG. 9. Comparison between the experimental D_2O TOF measurements and theory. The theory used a polar angle width of ∓2.5° and an azimuthal angle of ∓1°.

no sticking, experiments are performed at progressively lower temperatures. The scattered intensity is fairly constant until appreciable sticking commences. At the surface temperatures, where the intensity begins to much more rapidly decrease, there is a competition between adsorption and desorption. Initially, the scattered signal is nearly constant, but as the surface temperature is further decreased, the scattered signal slowly decreases over the course of the measurement. Figure 4(b) summarizes the experiments, showing the relative intensities and the difference between shutter open and closed as a function of T_S., clearly showing a region over the span of a few degrees K where the D_2O is beginning to appreciably stick. It is important to note that the relative intensities are not to be exactly equated to the sticking coefficient. This is because at the surface temperature where there is a change in the slope, which we attribute to the commencement of appreciable sticking, there is also slow but appreciable desorption. This is something we see using thermal desorption experiments. This is further demonstrated by using D_2O beams with the same translational energy but a different flux, to be discussed shortly. The higher flux beam shows initial sticking at a higher surface temperature, and we attribute this result to the larger quantity of adsorbed D_2O due to the greater impingement rate while the desorption stays relatively constant.

Figure 5 shows results for experiments where the incident energy is changed by a factor of two while the flux is nearly the same. Figure 5(a) shows some of the King and Wells results. It is evident that at T_S = 157 K, the E_I = 370 meV D_2O has a greater sticking coefficient. In addition, shown is the result for E_I = 370 meV and T_S = 159 K. This is nearly identical with the results for E_I = 728 meV and T_S = 157 K, indicating that this is the surface temperature where the two different beams have nearly identical sticking. Figure 5(b) summarizes the results. The different initial energy does affect the sticking. This would be consistent with the fact that it is less likely that a faster D_2O molecule will stick because it needs to exchange a larger amount of energy with the surface. However, this effect appears to be small—only about 2 K. In light of the TOF measurements to be described later in this paper showing that at these energies most of the scattered D_2O retains an appreciable amount of the incident energy, the sticking is due to relatively rare molecule-surface collision events, which lead to a much greater than average energy exchange.

Figure 6 shows the results of measurements where E_I was nearly the same but the flux was different by a factor of 2. Figures 6(a) and 6(b) show examples of the spectra for high and low flux respectively. At T_S = 152 K, the low flux D_2O beam shows little evidence of sticking, while the high flux beam is definitely showing decreased scattering. Again, this is probably consistent with a competition between adsorption and desorption. Figure 6(c) summarizes the results; the higher flux beam begins demonstrating sticking behavior at a slightly lower surface temperature.

Figure 7 shows the results for the surface temperature dependence of the D_2O sticking. The carrier gas was He, so both the total scattering of D_2O and the He specular scattering could be monitored simultaneously. Figure 7(a) shows the total D_2O scattering as a function of T_S, while Fig. 7(b) shows the He specular scattering. At T_S = 170 K, there is no sticking; the D_2O scattering intensity is constant, as is the He signal. When T_S is lowered to 160 K, the D_2O signal starts a slow decay, meaning that more D_2O is adsorbed with time. However, the He specular is initially constant before starting to decrease. One explanation for this behavior is that the initial nucleation sites are at defects in the surface; these sites would already be scattering He away from the surface. If further D_2O adsorption caused these initial sites to grow, they could spread onto the ordered surface and begin scattering He away from the specular direction. At T_S = 155 K, the D_2O scattering attenuates much faster, as does the He specular. However, the He signal curve has an inflection at about 150 s, and the slope becomes less steep. This is an indicator of some morphological change at the surface, likely due to the start of island formation as the reflectivity at first diminishes due to disorder and then recovers in this temperature and flux regime due to the formation of coherently scattering islands of adsorbates. This does not happen at lower temperatures due to decreased mobility and the ordering of adsorbed species. The simulations cannot inform this point yet, as they are only performed for the scattering of isolated, individual molecules. This phenomenon happens because the scattering cross-sections of the adsorbed molecules overlap as the islands form, so the effective scattering cross-section of each additional D_2O decreases.[8,13] Figure 7(c) shows the integrated TPD signal. We do

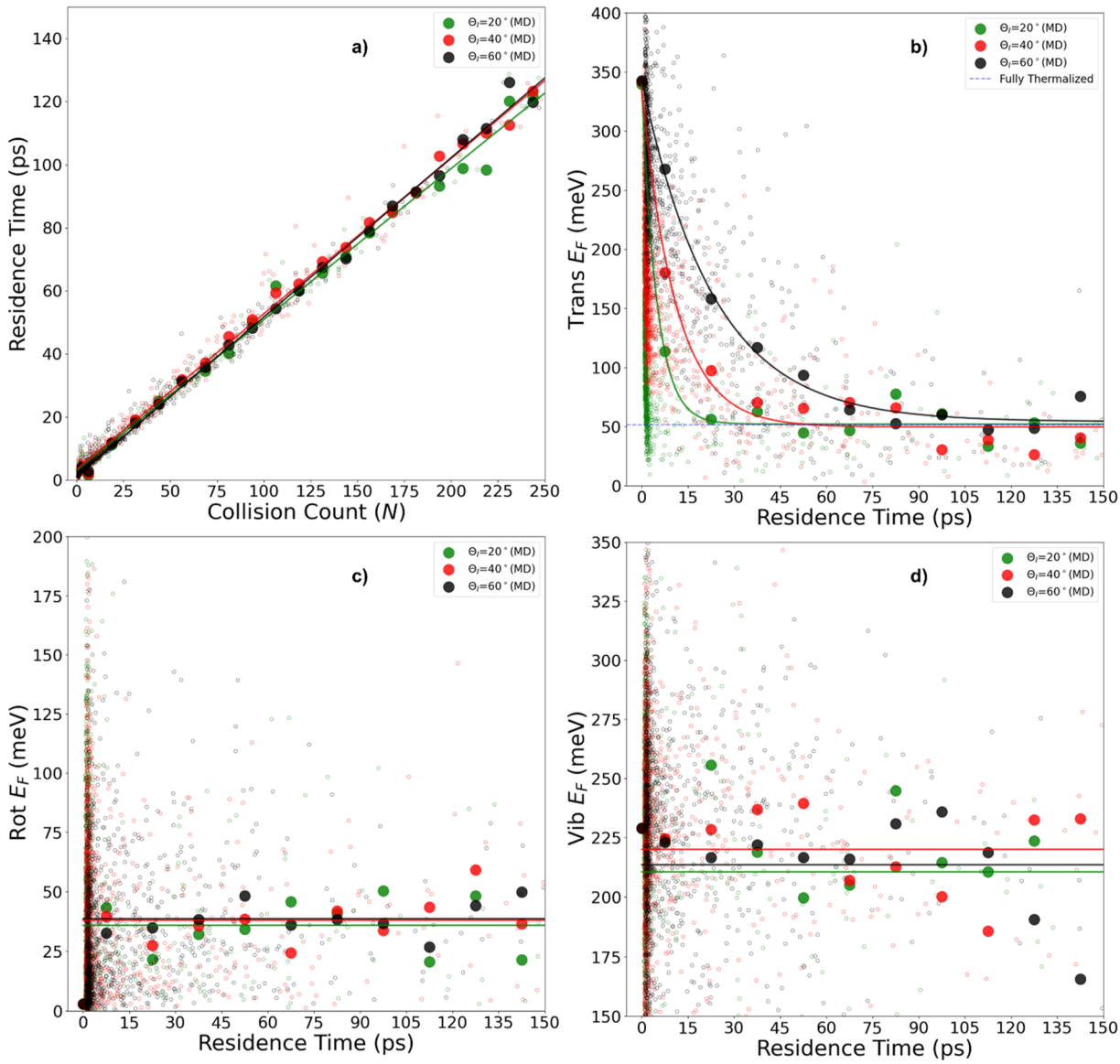

FIG. 10. Dynamics of D_2O on a HOPG surface. (a) The correlation between the residence time and the number of collisions. (b), (c), and (d): the translational, rotational, and vibrational energies of D_2O as a function of residence time. Small empty circles represent individual trajectories, while large solid circles denote average values. The line is the least absolute deviation fit of the average values.

not have an absolute measure of the quantity of adsorbed D_2O, but based on previous experiments, it is probable that the TPD signal corresponds to multilayer ice.[25] At T_S = 150 K, the D_2O signal rapidly decays, but the He specular curve is no longer monotonically decreasing; possibly it is the ice surface ordering. Since the TPD signal is experimentally identical at these and lower temperatures and the D_2O signal rapidly decreases to the background level, the sticking coefficient must be nearly unity.

For an impinging molecule to be adsorbed, it must exchange enough energy with the surface to be trapped in the gas–surface potential well. To better understand this dynamical process, we performed scattering experiments where both the angular intensity distribution and the scattered velocities were measured. The TOF measurements were performed with the post-chopper. Though unnecessary under the conditions of these experiments, the post-chopper allows us to separate actual flight times from surface

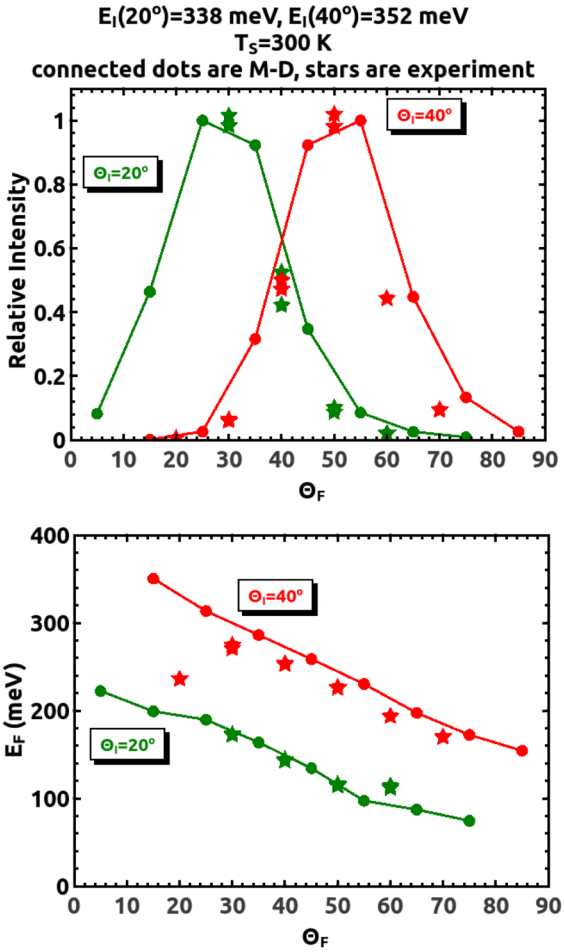

FIG. 11. Comparison between the experimental Ne TOF measurements and theory. The theory used a polar angle width of ∓2.5° and an azimuthal angle of ∓1°.

residence times. Most of the experiments were performed at a surface temperature well above any D_2O sticking. This eliminates the possibility of a fraction of the scattering being from D_2O-covered graphite rather than bare graphite. Examples of some TOF spectra are shown in Fig. 8. Included are lines from the least-squares fitting of the data. Figure 9 shows a comparison of the average final energy ($\langle E_F \rangle$) and relative intensity between the experimental results and the theory. There is excellent agreement. The principal departure between the measurements and prediction is the more normal Θ_F, where the scattered intensity is small. One explanation is that the HOPG has some defects, very probable over the ~1 mm beam spot size, and we know from our own experiments that sputter damaged HOPG has some higher energy scattering at Θ_F near normal.

Under most conditions, the scattered D_2O still retains an appreciable percentage of the incident energy. At T_S = 300 K, a thermalized molecule will leave the surface with $\langle E_F \rangle$ = 52 meV ($2 * k_B * T_S$, where k_B is Boltzmann's constant). This would be the expected $\langle E_F \rangle$ if the molecules had completely accommodated the surface and were most closely approached at the most normal incident angle, Θ_F = 20°. For the higher final energies, we could probably experimentally resolve direct-inelastic scattering and trapping-desorption, where the D_2O is transiently adsorbed and accommodates to the surface temperature. The trapped-desorbed molecules also leave the surface with a $\cos(\Theta_F)$ intensity distribution. There were only a few experimental spectra, taken near normal, where there may have been a hint of a trapping-desorption component.

The excellent agreement between experiments and simulations validates the trajectories, where the motions of atoms are followed at a femtosecond resolution, thus providing an ideal opportunity to probe into the nature of energy transfer between D_2O and the HOPG surface. The threshold of trapping-desorption is defined as those trajectories where D_2O collides with the HOPG surface more than once. The percentages of the trapping-desorption D_2O are 20%, 32%, and 48% for Θ_I of 20°, 40°, and 60°, respectively. This is due to the collision velocity (the component that is perpendicular to the HOPG surface) decreasing as Θ_I increases, and more D_2O is temporarily trapped. It is also of interest to note that the number of collisions has a good linear correlation with the residence time, which is defined as the time when D_2O is within 1.2 nm of the HOPG surface [Fig. 10(a)]. At this distance, the interaction between them is only 0.05% of the binding energy (ε in Table I). As Fig. 10(b) shows, the translation energy of D_2O (measured after desorption from the surface) decreases as the residence time increases, with a much faster decreasing rate early on (e.g., less than 15 ps). It is interesting to note the impact of Θ_I on the trapping-desorption of D_2O. On one hand, Θ_I has no impact on the asymptotic behavior of the translational energy of D_2O, as they all converge to the same level (52 meV), the average translational energy at 300 K, and the temperature of the HOPG surface. This result indicates that, with long enough residence time, D_2O eventually "forget" its initial state and is thermalized by the surface. On the other hand, those D_2O with a larger Θ_I (thus a smaller collision velocity) lose translational energy at a slower rate, aligning with the percentages of the trapping-desorption discussed earlier. This picture also correlates well with the translation energy of D_2O vs Θ_F (Fig. 9): D_2O moves slower and slower in the direction perpendicular to the HOPG surface as more collisions take place. This long-trapped D_2O eventually leaves the HOPG surface with a small velocity in the direction perpendicular to the surface, resulting in a large Θ_F. Although it is out of the scope of the simulation in this paper, this long-trapped D_2O could be important to the initial frozen event of the HOPG surface, as it has a higher chance of being stabilized by the collision of more water molecules. Collisions with the HOPG surface excite the rotational degree of freedom of D_2O [Fig. 10(c)] immediately, and it is interesting to note that although there are large fluctuations, the average value of the rotational energy of D_2O after collision shows it is thermalized (the average rotational energy of D_2O at 300 K is 39 meV). As expected, collisions with the HOPG surface do not excite the vibrational degrees of freedom of D_2O [Fig. 10(d)] because the surface temperature is low. Θ_I has no meaningful impact on the excitation of the internal degree of freedom of D_2O.

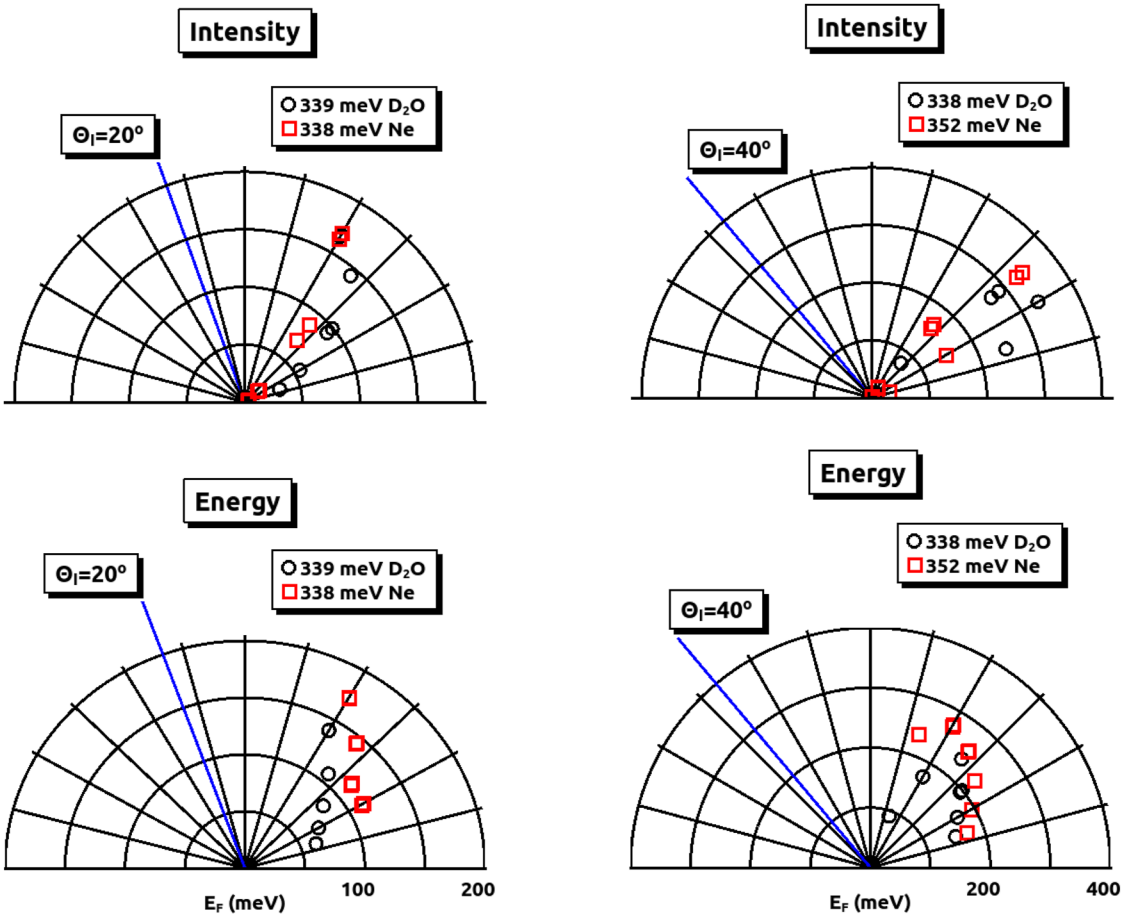

FIG. 12. Comparison between Ne and D_2O scattering under similar conditions. For intensity results, they are scaled by dividing the value of the maximum measured intensity.

Figure 11 shows the same experimental and theoretical comparison for Ne scattering. This gives results for the same mass but without any internal degrees of freedom. Again, the agreement is quite good. Figure 12 compares the scattering of D_2O and Ne under similar conditions. Besides the internal energy, the difference in the gas–surface well depth is ~40 meV for Ne[26] and ~100 meV for D_2O,[6] which might affect the scattering as the effective incident energy is changed by the depth of the potential well. From our simulations, we know that under these conditions, the average vibrational energy of the incident energy does not change, but the average rotational energy increases by ~40 meV. The TOF spectra show that the translational energy may be slightly lower for the D_2O. More striking is that the angular intensity distributions are shifted toward larger final angles for D_2O as compared with Ne.

The difference in the scattering dynamics observed in D_2O vs Ne simulations can be attributed to the difference in their interaction with the HOPG surface as well as the rotational excitation that is absent in Ne. As Table I shows, compared to D_2O, Ne has a much weaker interaction with the HOPG surface, resulting in only 1% trapping-desorption trajectories for both Θ_I (20° and 40°). For trapping-desorption Ne, the residence time is much smaller compared to D_2O. It is interesting to note that Θ_I has different impacts on the translational energy of trapping-desorption Ne, as Θ_I of 20° and 40° converge to different translational energies (Fig. 13). The reason for this phenomenon warrants further investigation, but our hypothesis is that (1), as seen in the D_2O case, the higher the collision velocity (e.g., the smaller Θ_I), the faster the loss of translation energy, and (2) there is not enough residence time for Ne to be thermalized.

Figure 14 shows the results of TOF measurements made at a surface temperature where D_2O does not stick (200 K) and surface temperatures where the sticking is just beginning. At the onset of sticking, the intensity decreases, as expected. Interestingly, $\langle E_F \rangle$ at $\Theta_F = 45°$ falls off more rapidly than $\langle E_F \rangle$ at $\Theta_F = 55°$, the more glancing final angle. Since this change occurs rather abruptly when sticking commences, it is likely that this is due to backscattering from adsorbed D_2O. We did not attempt to model this phenomenon.

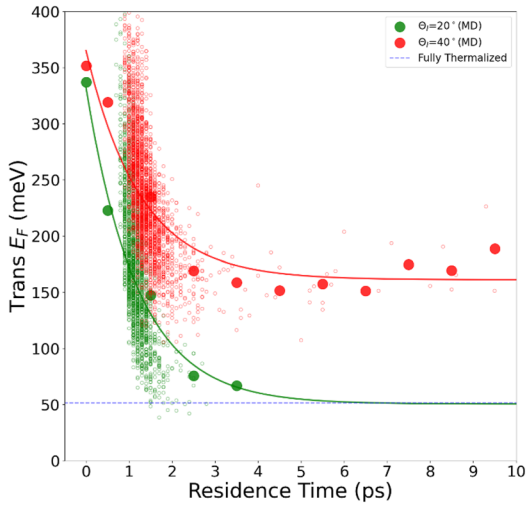

FIG. 13. Translational energy vs residence time of Ne. Small empty circles represent individual Ne trajectories, while large solid circles denote the average values. The line is the least absolute deviation fit of the average values.

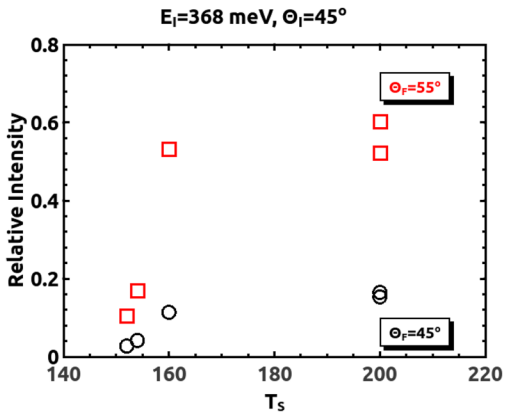

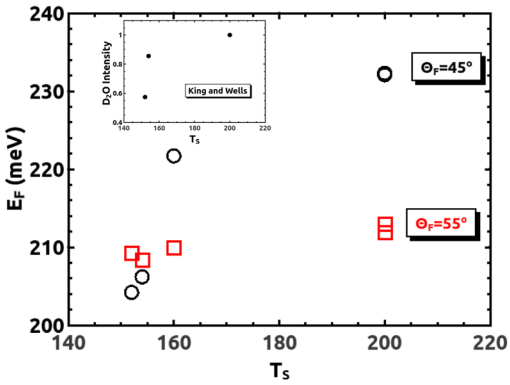

FIG. 14. Results of D_2O TOF measurements at $\Theta_I = 45°$ with two different Θ_F and different T_S. The inset is the King and Wells results to show the onset of D_2O sticking.

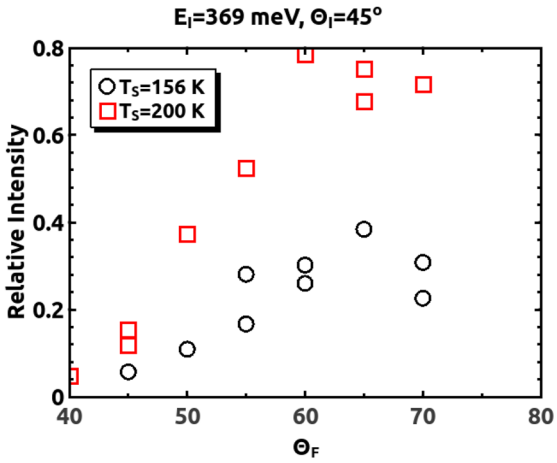

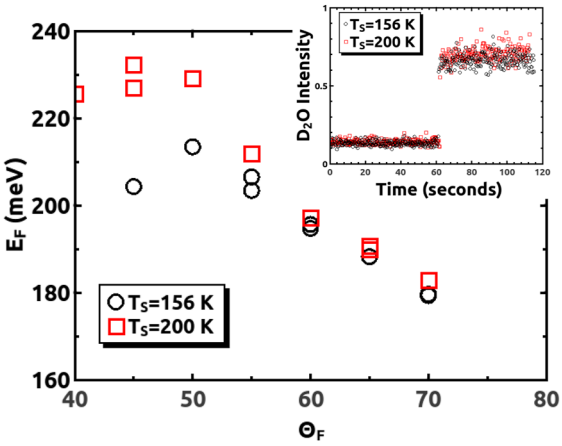

FIG. 15. Results of D_2O TOF measurements at $\Theta_I = 45°$ and different T_S. The inset shows the King and Wells results for the two different temperatures.

Figure 15 shows the results of experiments performed at two different surface temperatures, $T_S = 200$ K, where there is no D_2O sticking, and $T_S = 156$ K, where sticking is just getting started. Again, there is a decrease in the intensity at the lower temperature. At more glancing angles, the final energy is the same at the two different temperatures but is noticeably lower at the more normal final angles at $T_S = 156$ K as compared to $T_S = 200$ K. Again, this is consistent with in-plane backscattering of the incident molecules.

CONCLUSIONS

In this paper, we discuss our efforts to understand the mechanism by which water sticks to solid surfaces. Specifically, we used molecular beams containing D_2O impinging upon a ZYA HOPG graphite surface. The experiments were undertaken to understand the sticking of water with high translational energies, ~350–750 meV. The use of beam techniques allowed for control

of the beam energy, exact composition, and incident angle of the collision with the surface.

Under the conditions of our experiments, the initial sticking begins at a surface temperature of ~160 K. Based on the He specular scattering and thermal desorption experiments, at this temperature, the adsorption is random since the coverage is initially low. This is due to the low flux of D_2O in these beams; the coverage, therefore, remains low due to both the low incident flux and the appreciable desorption rates at these temperatures. The initial sticking temperature shows a slight energy dependence $\langle E_I \rangle$ between 370 and 730 meV, with the sticking occurring at ~2 K lower for the lower incident energy. This is probably due to the amount of energy that must be exchanged with the surface for trapping to occur. The flux also has a definite effect; a larger D_2O flux leads to a higher initial sticking temperature. This is a manifestation of the still appreciable desorption rate.

To examine the energy exchange with the surface, the first step in the sticking of these relatively fast D_2O molecules, we made time-of-flight measurements of scattered D_2O. We then compared these measurements with realistic theoretical simulations. The good agreement between theory and experiment allows us to extract information about the physics of the gas–surface interaction. One important take-home lesson is that a D_2O molecule has to interact with the surface for a relatively long time to lose enough energy to become thermalized with the surface, the point at which the molecules are at least transiently adsorbed. Some of the experiments did show a possible hint of some trapping-desorption. However, these molecules would be scattered over 2 pi steradians, not just in the scattering plane, making them even more difficult to experimentally detect, and the theory predicts this to be a minor component of the total scattered D_2O.

This study provides a fundamental understanding of gas–surface collisional energy exchange at temperatures above, nearing, and at condensation temperatures for gases incident under high-velocity non-equilibrium conditions onto a model substrate, HOPG graphite. In the future, we intend to extend these measurements to other surfaces that are more hydrophilic and hydrophobic than HOPG to further refine our understanding of the freezing of water onto surfaces. Such understanding is sought to help create interfaces with more highly controlled water sticking and condensation characteristics for many real-world applications such as airframe design and anti-icing texturing for windmill power generation.

ACKNOWLEDGMENTS

The authors gratefully acknowledge funding from the Air Force Office of Scientific Research Grant No. FA9550-19-1-0324, with focus on the dynamics of energetic gas–surface interactions; Grant No. FA9550-20-1-0351, with a focus on water and ice interactions at interfaces; and support for instrumentation from the AFOSR-DURIP program Grant No. FA9550-23-1-0528. The National Science Foundation, with a focus on interfacial chemical kinetics, is also gratefully acknowledged via Grant No. CHE-231336, as well as infrastructure support from the NSF-Materials Research Science and Engineering Center at the University of Chicago, MRSEC Grant No. DMR-2011854. The authors also acknowledge the Information and Technology Services (ITS) from the University of Hawai'i, Manoa, for the computational resources that enabled the simulations for this study.

AUTHOR DECLARATIONS

Conflict of Interest

The authors have no conflicts to disclose.

Author Contributions

Kevin D. Gibson: Formal analysis (equal); Investigation (equal); Methodology (equal); Writing – original draft (equal); Writing – review & editing (equal). **Yuheng Luo**: Formal analysis (equal); Investigation (equal); Methodology (equal); Software (equal); Writing – original draft (equal). **Christopher Kang**: Methodology (equal); Software (equal). **Rui Sun**: Formal analysis (equal); Funding acquisition (equal); Investigation (equal); Methodology (equal); Resources (equal); Software (equal); Writing – original draft (equal); Writing – review & editing (equal). **Steven J. Sibener**: Conceptualization (lead); Formal analysis (equal); Funding acquisition (lead); Project administration (lead); Supervision (lead); Writing – original draft (equal); Writing – review & editing (equal).

DATA AVAILABILITY

The data that support the findings of this study are available within the article.

REFERENCES

[1] *Nucleation Water*, edited by A. Laaksonen and J. Malila (Elsevier, 2022), pp. i–iii.
[2] A. Clemens, L. Hellberg, H. Gronbeck, and D. Chakarov, "Water desorption from nanostructured graphite surfaces," Phys. Chem. Chem. Phys. **15**(47), 20456–20462 (2013).
[3] M. J. Stirniman, C. Huang, R. Scott Smith, S. A. Joyce, and B. D. Kay, "The adsorption and desorption of water on single crystal MgO(100): The role of surface defects," J. Chem. Phys. **105**(3), 1295–1298 (1996).
[4] Y. Segal, A. Khain, M. Pinsky, and A. Sterkin, "Sensitivity of raindrop formation in ascending cloud parcels to cloud condensation nuclei and thermodynamic conditions," Q. J. R. Metereol. Soc. **130**(597), 561–581 (2004).
[5] A. Kozbial, F. Zhou, Z. Li, H. Liu, and L. Li, "Are graphitic surfaces hydrophobic?," Acc. Chem. Res. **49**(12), 2765–2773 (2016).
[6] J. G. Brandenburg, A. Zen, M. Fitzner, B. Ramberger, G. Kresse, T. Tsatsoulis, A. Grüneis, A. Michaelides, and D. Alfè, "Physisorption of water on graphene: Subchemical accuracy from many-body electronic structure methods," J. Phys. Chem. Lett. **10**(3), 358–368 (2019).
[7] M.-L. Tao, K. Sun, X. Zhang, L.-J. Zhao, D.-X. Yang, Z.-L. Wang, and J.-Z. Wang, "Direct observation of the water dimer adsorbed on graphite," Appl. Surf. Sci. **505**, 144600 (2020).
[8] B. Poelsema and G. Comsa, *Scattering of Thermal Energy Atoms from Disordered Surfaces* (Springer-Verlag, Berlin, Heidelberg, New York, 1989).
[9] D. King and M. Wells, "Molecular-beam investigation of adsorption kinetics on bulk metal targets: Nitrogen on tungsten," Surf. Sci. **29**(2), 454–482 (1972).
[10] N. Miyoshi, K. Osuka, I. Kinefuchi, S. Takagi, and Y. Matsumoto, "Molecular beam study of the scattering behavior of water molecules from a graphite surface," J. Phys. Chem. A **118**(26), 4611–4619 (2014).
[11] N. Marković, P. U. Andersson, M. B. Någård, and J. B. C. Pettersson, "Scattering of water from graphite: Simulations and experiments," Chem. Phys. **247**(3), 413–430 (1999).

[12]K. D. Gibson, D. R. Killelea, H. Yuan, J. S. Becker, and S. J. Sibener, "Determination of the sticking coefficient and scattering dynamics of water on ice using molecular beam techniques," J. Chem. Phys. **134**(3), 034703 (2011).
[13]B. Poelsema, R. L. Palmer, and G. Comsa, "A thermal He scattering study of CO adsorption on Pt(111)," Surf. Sci. Lett. **136**(1), 1–14 (1984).
[14]W. L. Jorgensen, D. S. Maxwell, and J. Tirado-Rives, "Development and testing of the OPLS all-atom force field on conformational energetics and properties of organic liquids," J. Am. Chem. Soc. **118**(45), 11225–11236 (1996).
[15]M. Majumder, H. N. Bhandari, S. Pratihar, and W. L. Hase, "Chemical dynamics simulation of low energy N_2 collisions with graphite," J. Phys. Chem. C **122**, 612 (2018).
[16]W. L. Hase, N. Date, L. B. Bhuiyan, and D. G. Buckowski, "Energy transfer in collisions of argon with highly excited water and methane," J. Phys. Chem. **89**(12), 2502–2507 (1985).
[17]B. R. Brooks, R. E. Bruccoleri, B. D. Olafson, D. J. States, S. Swaminathan, and M. Karplus, "CHARMM: A program for macromolecular energy, minimization, and dynamics calculations," J. Comput. Chem. **4**(2), 187–217 (1983).
[18]E. Neria, S. Fischer, and M. Karplus, "Simulation of activation free energies in molecular systems," J. Chem. Phys. **105**(5), 1902–1921 (1996).
[19]R. Ramírez and C. P. Herrero, "Quantum path-integral study of the phase diagram and isotope effects of neon," J. Chem. Phys. **129**(20), 204502 (2008).
[20]X. Hu, W. L. Hase, and T. Pirraglia, "Vectorization of the general Monte Carlo classical trajectory program VENUS," J. Comput. Chem. **12**(8), 1014–1024 (1991).
[21]W. L. Hase, R. J. Duchovic, X. Hu, A. Komornicki, K. F. Lim, D.-H. Lu, G. H. Peslherbe, K. N. Swamy, S. R. Vande Linde, A. Varandas, H. Wang, and R. J. Wolf, "A general chemical dynamics computer program," Quantum Chem. Program Exch. **12**, 671 (1996).
[22]M. J. Abraham, T. Murtola, R. Schulz, S. Páll, J. C. Smith, B. Hess, and E. Lindahl, "GROMACS: High performance molecular simulations through multi-level parallelism from laptops to supercomputers," SoftwareX **1–2**, 19–25 (2015).
[23]G. Bussi, D. Donadio, and M. Parrinello, "Canonical sampling through velocity rescaling," J. Chem. Phys. **126**(1), 014101 (2007).
[24]W. F. Van Gunsteren and H. J. C. Berendsen, "A leap-frog algorithm for stochastic dynamics," Mol. Simul. **1**(3), 173–185 (1988).
[25]Y. Luo, K. Fujioka, A. Shoji, W. L. Hase, K.-M. Weitzel, and R. Sun, "Theoretical study of the dynamics of the $HBr^+ + CO_2 \rightarrow HOCO^+ + Br$ reaction," J. Phys. Chem. A **124**(44), 9119–9127 (2020).
[26]M. Abbaspour, H. Akbarzadeh, S. Salemi, and M. Sherafati, "Molecular dynamics simulation of noble gas adsorption on graphite: New effective potentials including many-body interactions," J. Mol. Liq. **222**, 915–922 (2016).